Kinetic Analysis of ^{18}F-fluorodihydrorotenone as a Deposited Myocardial Flow Tracer: Comparison to Thallium-201

Robert C. Marshall, MD; Patricia Powers-Risius, BA; Bryan W. Reutter, MS; James P. O'Neil, PhD; Michael La Belle, PhD; Ronald H. Huesman, PhD; and Henry F. VanBrocklin, PhD

Department of Nuclear Medicine and Functional Imaging
E. O. Lawrence Berkeley National Laboratory
University of California
Berkeley, CA 94720

Address correspondence and reprint requests to:
Bryan W. Reutter, Dept. of Nuclear Medicine and Functional Imaging
Lawrence Berkeley National Laboratory
University of California
1 Cyclotron Road, MS55–121
Berkeley, CA 94720
Phone: 510-486-4265; FAX: 510-486-4768; E-mail: bwreutter@lbl.gov

First Author:
Dr. Robert C. Marshall, Dept. of Nuclear Medicine and Functional Imaging
Lawrence Berkeley National Laboratory
University of California
1 Cyclotron Road, MS55–121
Berkeley, CA 94720
Phone: 510-486-6537; FAX: 510-486-4768; E-mail: rcmarshall@lbl.gov

This study was supported by National Heart, Lung, and Blood Institute Grants PO1 HL25840 and RO1 HL6087701 and by the Director, Office of Science, Office of Biological and Environmental Research (OBER), Medical Science Division of the United States Department of Energy under OBER contract DE–AC03–76SF00098.

Abbreviated Title: Fluorodihydrorotenone as a Flow Tracer.

Abbreviated Title: Fluorodihydrorotenone as a Flow Tracer

ABSTRACT

The goal of this investigation was to assess the accuracy of ^{18}F-fluorodihydrorotenone (^{18}F-FDHR) as a new deposited myocardial flow tracer and compare the results to those for ^{201}Tl. **Methods**. The kinetics of these flow tracers were evaluated in 22 isolated, erythrocyte- and albumin-perfused rabbit hearts over a flow range encountered in patients. The two flow tracers plus a vascular reference tracer (^{131}I-albumin) were introduced as a bolus through a port just above the aortic cannula. Myocardial extraction, retention, washout, and uptake parameters were computed from the venous outflow curves using the multiple indicator dilution technique and spectral analysis. **Results**. The mean initial extraction fractions of ^{18}F-FDHR (0.85 ± 0.07) and ^{201}Tl (0.87 ± 0.05) were not significantly different, although the initial extraction fraction for ^{18}F-FDHR declined with flow ($P < 0.0001$), whereas the initial extraction fraction of ^{201}Tl did not. Washout of ^{201}Tl was faster ($P < 0.001$) and more affected by flow ($P < 0.05$) than ^{18}F-FDHR washout. Except for initial extraction fraction, ^{18}F-FDHR retention was greater ($P < 0.001$) and less affected by flow ($P < 0.05$) than ^{201}Tl retention. Reflecting its superior retention, net uptake of ^{18}F-FDHR was better correlated with flow than ^{201}Tl uptake at both one and fifteen minutes after tracer introduction ($P < 0.0001$ for both comparisons). **Conclusion**. The superior correlation of ^{18}F-FDHR uptake with flow indicates that it is a better flow tracer than ^{201}Tl in the isolated rabbit heart. Compared to the other currently available positron-emitting flow tracers (^{82}Rb, ^{13}N-ammonia, and ^{15}O-water), ^{18}F-FDHR has the potential of providing excellent image resolution without the need for an on-site cyclotron.

Key words: myocardial perfusion, fluorodihydrorotenone, PET

INTRODUCTION

Incomplete extraction and retention of ^{201}Tl and ^{99m}Tc-labeled flow tracers contribute to diagnostic and prognostic uncertainties in SPECT myocardial perfusion imaging (*1-5*). Although ^{82}Rb, ^{13}N-ammonia and ^{15}O-water can be used with PET to assess myocardial perfusion (*6-9*), problems with image resolution or the need for an on-site cyclotron has discouraged their widespread use. In an effort to find better perfusion indicators, we have been evaluating radiolabeled rotenone compounds as deposited myocardial flow tracers. Rotenone is a neutral, lipophilic compound that binds to complex I of the mitochondrial electron transport chain (*10-13*). We recently reported that ^{125}I-iodorotenone was superior to ^{99m}Tc-sestamibi as a deposited flow tracer in the isolated rabbit heart (*14*).

In this investigation, a second radiolabeled rotenone analogue, ^{18}F-fluorodihydrorotenone (^{18}F-FDHR), was evaluated as a potential myocardial flow tracer, comparing it to ^{201}Tl instead of ^{99m}Tc-sestamibi. The experimental preparation was the isolated, isovolumic rabbit heart perfused retrograde with red blood cells (RBC) and bovine serum albumin (BSA). ^{18}F-FDHR and ^{201}Tl kinetics were assessed at flow rates ranging from 0.3 to 3.5 mL/min/g of left ventricular (LV) wet weight. Myocardial tracer deposition was determined from venous outflow curves after bolus introduction of ^{18}F-FDHR, ^{201}Tl, and the intravascular tracer, ^{131}I-albumin. Initial extraction fraction, net retention, washout and net uptake of both flow tracers were computed using the multiple indicator dilution technique and spectral analysis (*14-16*). Spectral analysis allowed separation of extravascular from intravascular tracer distribution and was also used in our previous report comparing ^{125}I-iodorotenone and ^{99m}Tc-sestamibi (*14*). Since experimental protocols and data analysis were identical in these two studies, it is possible to compare results for all four flow tracers.

Our results indicate that ^{18}F-FDHR and ^{201}Tl were equally well extracted during the initial peak of the venous outflow curves. However, net retention and uptake of ^{18}F-FDHR were greater than ^{201}Tl for the remainder of the 15-min experiment, making ^{18}F-FDHR superior to ^{201}Tl as a deposited flow tracer in the isolated rabbit heart. Combining the results of both studies, the two radiolabeled-rotenone analogues had first-pass extraction fractions comparable to ^{201}Tl and better retention than ^{99m}Tc-sestamibi for at least 15 min after tracer introduction, making ^{18}F-FDHR and ^{125}I-iodorotenone better flow tracers in the isolated rabbit heart. If similar results were observed in patients, ^{123}I-rotenone could be used with SPECT and ^{18}F-FDHR with PET for a more accurate assessment of regional myocardial perfusion during stress and at rest.

MATERIALS AND METHODS

Experimental Preparation

All procedures were performed according to institutional guidelines for animal research. Preparation of isovolumic, retrograde RBC- and albumin-perfused rabbit hearts (n = 22*)* was similar to previous reports (*14, 17*). Hearts were obtained from male New Zealand rabbits (R&R Rabbitry, Stanwood, WA) weighing approx. 4 kg. The perfusate buffer was a modified Tyrode's solution containing 22 g/L BSA (Fraction V, fatty-acid free, Roche Diagnostics, Indianapolis, IN), and oxygenated bovine RBCs adjusted to a hematocrit level of 17–20%. Substrates were 5 mmol/L glucose and 2 mmol/L sodium pyruvate. Electrolyte concentrations were (in mmol/L): 110 for NaCl, 2.5 for $CaCl_2$, 6 for KCl, 1 for $MgCl_2$, 0.435 for NaH_2PO_4, and 28 for $NaHCO_3$. The pH and oxygen tensions were measured using an IRMA™ Blood Gas Analyzer (Diametrics Medical, Inc., St. Paul, MN). The mean (± SD) pH value was 7.44 ± 0.06 and the partial pressure of oxygen was 320 ±

127 mm Hg. To maintain oxygenation and a stable pH, the surface of the RBC-containing perfusate was equilibrated with a mixture of 98% O_2 and 2% CO_2 during the experiment.

After a rabbit was given 4000 U heparin (Upjohn, Kalamazoo, MI) and 250 mg pentobarbital sodium (Abbott, North Chicago, IL) through an ear vein, the heart was excised through a median sternotomy, arrested in ice-cold saline, and attached to a cannula to allow retrograde perfusion. After inserting an apical drain into the left ventricle, a fluid-filled latex balloon connected to a Gould-Statham P23ID pressure transducer (Gould, Oxnard, CA) was inserted across the mitral valve into the LV cavity. Perfusion pressure and systolic and diastolic ventricular pressures were recorded continuously on a Graphtec Linearecorder (Western Graphtec, Irvine, CA). A coronary venous sampling catheter and needle thermistor (Omega Engineering, Inc., Stamford, CT) were inserted into the right ventriclar cavity across the tricuspid valve. The venae cavae and pulmonary artery were ligated so all coronary venous drainage flowed out of the sampling catheter. The atrioventricular node was crushed to allow controlled stimulation using 4-V, 4-ms stimuli from a Grass SD44 stimulator. Temperature was maintained between 36°C and 38°C with a water-jacketed heating coil and heart chamber. Coronary flow was held constant with a peristaltic pump (Rainin Instruments, Woburn, MA). Coronary blood flow rate was measured by timed collection from the venous sampling catheter. The perfusate was not recirculated. Hearts were allowed to equilibrate for 15 min after surgical preparation was complete. During equilibration, developed pressure (peak systolic minus diastolic) was stable and averaged 73 ± 14 mm Hg.

Experimental Protocol

After equilibration, myocardial perfusion was gradually changed to the experimental flow rate and subsequently held constant by the perfusion pump. Twenty-two hearts were evaluated. Each heart was studied at only one flow rate, ranging from 0.3 to 3.5 mL/min/g of LV wet weight. Balloon volume and stimulus rate remained constant throughout all experiments. After 10 min at the experimental flow rate, a mixed isotope bolus consisting of ^{131}I-albumin (0.14 μCi), ^{18}F-FDHR (4.6 μCi), and ^{201}Tl (0.32 μCi) was injected just above the aortic cannula in 0.2 mL perfusate buffer containing BSA but no RBCs. Venous sampling was performed as previously described (*14, 18*).

Radiopharmaceuticals

Thallium-201 was purchased from Mallinkrodt Medical, San Francisco, CA. Bovine serum albumin was labeled with ^{131}I (DuPont-NEN Research Products) using the IODO-GEN-based protein iodination technique (*19*).

High specific activity fluorine-18 was prepared by the ^{18}O(p,n) ^{18}F reaction with 10 MeV protons from the LBNL Biomedical Isotope Facility CTI RDS 111 cyclotron on ^{18}O enriched water. The aqueous ^{18}F-fluoride ion was azeotropically dried with acetonitrile under a gentle stream of nitrogen in the presence of tetra-n-butyl ammonium hydroxide to form reactive tetra-n-butyl ammonium ^{18}F-fluoride (TBA^{18}F). Nucleophilic displacement of the tosylate moiety of 7'-tosyloxy-6',7'-dihydroroten-12-ol (DHR-ol-OTs) with ^{18}F-fluoride ion (TBA^{18}F in acetonitrile for 20 min at 100°C) provided the 7'-[^{18}F]fluoro-6', 7'-dihydroroten-12-ol (^{18}F-FDHR-ol). The crude reaction mixture was filtered through a short plug of silica with ethyl acetate to remove unreacted ^{18}F-fluoride and the solvent was removed at 100°C under a stream of nitrogen.

^{18}F-FDHR-ol was oxidized with MnO_2 in a slurry of celite and dichloromethane to provide 7'-[^{18}F]fluoro-6', 7'-dihydrorotenone (^{18}F-FDHR). The reaction was filtered through celite, diluted with HPLC solvent and purified by HPLC (Partisil M9 25, 25% ethyl

acetate/75% hexanes, 6 mL/min). The product fraction was isolated and the solvent removed at 100°C under a stream of nitrogen and brought up in ethanol. The radiochemical purity was >99%.

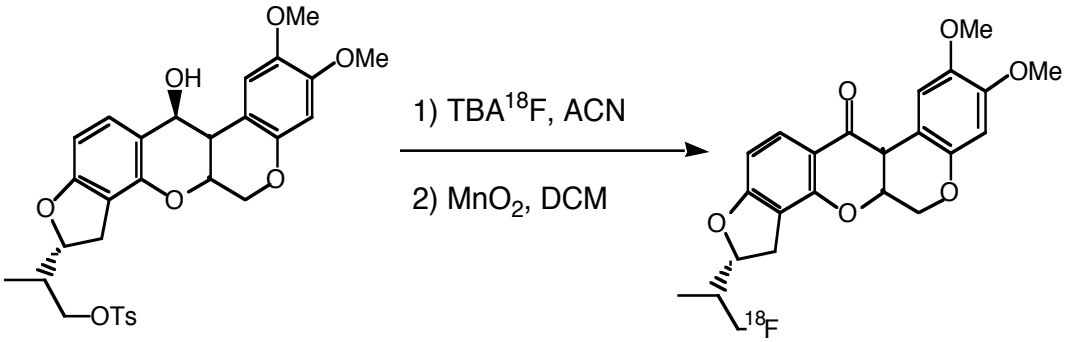

DHR-ol-OTs **^{18}F-FDHR**

Red Blood Cell Uptake and Albumin Binding

Binding studies of ^{18}F-FDHR and ^{201}Tl to RBCs were conducted at 37°C in the presence and absence of BSA. The hematocrit was 21% and the concentration of BSA was 2.2% (w/v). In the first set of experiments (n = 3), ^{18}F-FDHR, ^{201}Tl, RBCs, and BSA were incubated together in buffer. In the second set of experiments (n = 3), ^{18}F-FDHR and ^{201}Tl were incubated in buffer with RBCs but without BSA. Aliquots from both experimental series were removed and briefly centrifuged (15–20 s at 16,000 x g) to pellet the RBCs at various times (30 s to 15 min) after addition of the two perfusion tracers. The relative binding of ^{18}F-FDHR and ^{201}Tl to RBCs was determined by counting the cell pellet and supernatent (plus or minus albumin). In experiments with BSA, the minimal amount of ^{18}F-FDHR and ^{201}Tl bound to BSA was determined by precipitating the BSA with trichloroacetic acid (TCA) to a final concentration of 10%, and counting the protein pellet and supernatent separately.

Data Acquisition and Data Analysis

Venous samples and aliquots of a dilution of the isotope injection solution were counted on a gamma counter as previously described (*18*). Myocardial deposition kinetics of ^{18}F-FDHR and ^{201}Tl were assessed from the measured venous activity. The venous activity was expressed as a fractional venous appearance rate, h(t), and computed as:

$$h(t) = \frac{FC_i(t)}{Q_0} \qquad \text{Eq. 1}$$

where F denotes the blood flow (mL/s), $C_i(t)$ denotes the venous sample activity (cps/g), and Q_0 denotes the injected activity (cps). Physically, h(t) is a transport function that is determined by intravascular transport and dispersion in addition to bi-directional diffusion into and out of the extravascular space.

The multiple indicator dilution technique (*15*) and spectral analysis (*16*) were used to assess blood-tissue exchange of ^{18}F-FDHR and ^{201}Tl. The fundamental assumption of the multiple indicator dilution technique is that the intravascular reference tracer (^{131}I-albumin) accurately measures intravascular ^{18}F-FDHR and ^{201}Tl transport and dispersion. Based on this assumption, the differences between the ^{131}I-albumin venous concentration curve and

the curves for ^{18}F-FDHR and ^{201}Tl are used to measure transit time delays due to movement of the two flow tracers into and out of the extravascular space.

Mathematical analysis was based on a linear systems approach that assumes that: 1) the distribution of transit times for all three tracers does not change with time; 2) there is no interaction between tracer concentrations of radiolabeled reference and perfusion molecules; and 3) the uptake of any one perfusion tracer molecule does not influence the uptake of any other perfusion tracer molecule. Using this formalism, each perfusion tracer in the venous output of the heart was modeled as a convolution of the appearance of the intravascular reference tracer with a unit impulse response function. The unit impulse response function is the diffusible tracer venous concentration curve that would be observed following an idealized bolus without circulatory dispersion or transport delay. Physically, the impulse response function measures bi-directional diffusion into and out of the extravascular space after condensing intravascular transport and dispersion into an undelayed, narrow spike.

Spectral analysis quantifies ^{18}F-FDHR and ^{201}Tl extravascular transit time delays by producing a spectrum of kinetic components that describe each flow tracer's unit impulse response function. The impulse response function was computed by deconvolving the perfusion tracer venous concentration curves by the intravascular reference tracer (^{131}I-albumin) venous concentration curve. A non-negative weighted least squares algorithm was used to model the diffusible tracer fractional venous appearance rate, $h_D(t)$, as having one component that behaves like the reference tracer, $h_R(t)$, along with delayed components that can each be represented as the convolution of the reference tracer curve with a decaying exponential:

$$h_D(t) = h_R(t) * i(t) \equiv \int_0^t h_R(\tau) i(t-\tau) d\tau \qquad \text{Eq. 2}$$

where the unit impulse response function is:

$$i(t) = c_0 \delta(t) + \sum_{j=1}^{n} \frac{c_j}{t_j} e^{-t/t_j} \qquad \text{Eq. 3}$$

and $\delta(t)$ is the Dirac delta function that yields the undelayed component that behaves like the reference tracer. This component contains the fraction c_0 of injected activity that never escaped into the extravascular space. Extrapolating the spectral model to infinite time, the jth-delayed component contains a fraction c_j of the injected activity that has a mean transit delay time of t_j due to bi-directional diffusion between vascular and extravascular spaces.

A total of 100 non-negative components were used, with exponential time constants ranging between 1 s and 190 min equally spaced on a logarithmic scale. The extrapolated spectral component fractions were not constrained to add up to one due to the relatively short time frame of the experiments (15 min) compared to the mean transit time of the slowest possible spectral component (190 min). Given m positive delayed components indexed according to increasing mean transit delay time, the first m – 1 components were termed intermediate components and the mth component was termed the slow component. Using this kinetic model, the extraction fraction (D_0) for a diffusible tracer is:

$$D_0 = 1 - c_0 \qquad \text{Eq. 4}$$

and the combined fraction and combined mean transit delay time for the intermediate components are:

$$\left(c_{1,\ldots,m-1}, t_{1,\ldots,m-1}\right) = \left(\sum_{j=1}^{m-1} c_j, \frac{\sum_{j=1}^{m-1} c_j t_j}{\sum_{j=1}^{m-1} c_j} \right). \qquad \text{Eq. 5}$$

The deconvolved net tracer retention, $E_{net}(t)$, at time t is:

$$E_{net}(t) = 1 - \int_0^t i(\tau)d\tau = 1 - c_0 - \sum_{j=1}^{m} c_j\left(1 - e^{-t/t_j}\right). \qquad \text{Eq. 6}$$

The deconvolved fractional escape rate, FER(t), a measure of tracer washout, was calculated as the ratio of the delayed components of the impulse response and the deconvolved net tracer retention, for $t > 0$:

$$FER(t) = \frac{i(t)}{E_{net}(t)} = \frac{\sum_{j=1}^{m} \frac{c_j}{t_j} e^{-t/t_j}}{1 - c_0 - \sum_{j=1}^{m} c_j\left(1 - e^{-t/t_j}\right)} . \qquad \text{Eq. 7}$$

Net tissue tracer uptake, U(t), was computed as the product of tracer delivery by way of myocardial blood flow and net tracer retention:

$$U(t) = F \cdot E_{net}(t). \qquad \text{Eq. 8}$$

Net tissue tracer uptake provides a measure of extravascular tissue tracer content and is the best index of the ability of a perfusion tracer to accurately report flow (e.g., for an ideal tracer with an E_{net} of one over all times and flows, U(t) is equal to flow).

Statistics

Data are expressed as the mean ± SD. Statistical analyses were performed with the use of StatView statistical software (Abacus Concepts, Berkeley, CA) and the MATLAB Statistics Toolbox (MathWorks, Natick, MA). Regression lines were obtained using the unweighted least squares method. A t test was used to test hypotheses about the slopes and y-intercepts of individual regression lines. Welch's procedure (*20*) was used to compare the slopes of regression lines and to compare the areas under uptake-vs.-flow curves. Paired comparisons of kinetic parameters of ^{18}F-FDHR and ^{201}Tl were made using both a paired t test and a nonparametric Wilcoxon signed rank test. In all cases, the two tests yielded similar results regarding the statistical significance of the differences, and the larger of the two P values is reported. $P < 0.05$ was considered statistically significant.

RESULTS

RBC and Albumin Binding

Both bovine RBCs and BSA bound ^{18}F-FDHR. Without BSA, the rate with which RBCs bound ^{18}F-FDHR was rapid: the 30-s incubation showed that 90.5% ± 0.6% of the ^{18}F-FDHR was RBC-associated and that this value did not change significantly over 15 min. The average value across all time points was 90.5% ± 0.5%. As with RBCs alone, the binding of ^{18}F-FDHR to RBCs in the presence of BSA was also rapid with steady-state binding present following 30-s incubation. However, in the presence of BSA the binding of ^{18}F-FDHR to RBCs declined to an average across all time points of 37.7% (± 2.1%). When BSA from the RBC supernatent was precipitated with tricholoracetic acid,

equilibration between free and BSA-bound ^{18}F-FDHR was present after 30 s of incubation, with an average of 98.9% (± 1.4%) of total ^{18}F-FDHR activity associated with albumin.

In contrast to the ^{18}F-FDHR results, the rate with which ^{201}Tl bound to RBCs was much slower, requiring approx. 15 min (with or without BSA) to reach a constant value. The presence of BSA resulted in an initial increase in RBC-associated ^{201}Tl compared to RBCs without BSA. However, by 15 min, RBCs incubated with or without BSA reached the same levels, binding 55.2% (± 0.1%) of the total ^{201}Tl without BSA vs. 55.4% (± 0.4%) with BSA. Also, in contrast to the ^{18}F-FDHR results where virtually all the ^{18}F-FDHR in the supernatent was albumin-bound, only 47.7% (± 1.7%) of the ^{201}Tl present in the supernatent was bound to albumin at 15 minutes.

Myocardial Tracer Transport and the Impulse Response Function

Panel A in Figure 1 shows the concentration-time curves, expressed as fractional venous appearance rates, for ^{18}F-FDHR, ^{201}Tl, and ^{131}I-albumin from one experiment. Although introduced as a compact bolus, transport through the myocardium and associated perfusion tubing resulted in considerable temporal dispersion of the three tracers. For the intravascular tracer, the fractional venous appearance rates reflected the distribution of transit times through the myocardial vasculature as well as the inflow and outflow tubing. For the two diffusible flow tracers, some molecules remained in the vasculature with the same transit time distribution as the intravascular tracer. Other molecules escaped into the extravascular space where they either remained trapped for the duration of the experiment or diffused back into the vascular space. Escape of the two perfusion tracers out of the vascular space is evident from their lower fractional venous appearance rates during the initial peak of the venous concentration curves. Subsequent re-entry of the two perfusion tracers is seen during the later portions of the curves when their fractional venous appearance rates exceed the rate for the intravascular tracer.

The delayed components of the impulse response function for the first two min of this experiment are displayed in Panel B of Figure 1. These delayed components are the sum of decaying exponentials from Equation 3 and depict the distribution of transit time delays due to movement of flow tracer into the extravascular space followed by back diffusion into the intravascular space. For this experiment, a greater amount of ^{201}Tl re-entered the vascular space, indicating that more extracted ^{201}Tl diffused out of this heart than ^{18}F-FDHR during the first 120 s after tracer introduction.

The undelayed component fractions, c_0 , of the impulse response function for this experiment were 0.13 for ^{18}F-FDHR and 0.14 for ^{201}Tl (data not shown). These were the fractions of flow tracer molecules that remained inside the vasculature with transit time distributions indistinguishable from ^{131}I-albumin.

Spectral Analysis

As was the case with spectral analysis of data for ^{125}I-iodorotenone and ^{99m}Tc-sestamibi reported previously (*14*), there was consistency between measured and modeled fractional venous appearance curves for ^{18}F-FDHR and ^{201}Tl. Modeled diffusible tracer fractional venous appearance curves were obtained by convolving the measured ^{131}I-albumin reference curve with the impulse responses given by the spectral models. The average root mean square differences between measured and modeled data were normalized by the root mean square values of measured data samples and expressed as percentages. For the 22 experiments, these differences averaged 9.7% (± 6.0%) for ^{18}F-FDHR and 3.1% (± 2.6%) for ^{201}Tl.

A second similarity to previously reported data (*14*) was that some spectral model parameters exhibited variability (Table 1). The number of delayed components, m, in the impulse responses ranged from 1 to 4 for ^{18}F-FDHR and from 2 to 5 for ^{201}Tl. For each experiment, the number of ^{18}F-FDHR components was less than or equal to the number of ^{201}Tl components. On average, ^{18}F-FDHR models contained 3.3 delayed components and ^{201}Tl models contained 4.3 delayed components. However, despite this variability, robust estimates of extraction fraction, net retention, and washout (Eq. 4, 6 and 7, respectively) were obtained by evaluating the impulse response function (Eq. 3) and its integral.

Two notable trends in the spectra were that the combined fraction of intermediate components, $c_{1,\ldots,m-1}$, was significantly smaller for ^{18}F-FDHR than for ^{201}Tl ($P < 0.002$), and that the slow component mean transit delay time, t_m, was significantly greater for ^{18}F-FDHR than for ^{201}Tl ($P < 0.002$). Thus, the results obtained with the spectral model indicated that less ^{18}F-FDHR washed out in the 1–3 min intermediate time frame and long term retention of ^{18}F-FDHR was also better.

^{18}F-FDHR and ^{201}Tl Extraction

Figure 2 shows the initial extraction fraction (Eq. 4) values of ^{18}F-FDHR and ^{201}Tl as a function of myocardial blood flow for all 22 experiments. Over the range of flows evaluated, there was no significant difference between the mean initial extraction fraction of ^{18}F-FDHR (0.85 ± 0.07) and ^{201}Tl (0.87 ± 0.05) ($P > 0.1$). The initial extraction fraction for ^{18}F-FDHR decreased with flow ($P < 0.0001$), whereas flow did not have a significant effect on the initial extraction fraction for ^{201}Tl ($P > 0.2$).

^{18}F-FDHR and ^{201}Tl Washout

Figure 3 is a three-dimensional illustration or "surface-plot" of the effect of both time and flow on ^{18}F-FDHR and ^{201}Tl washout as quantified by fractional escape rate [FER(t), Eq. 7]. The surface height represents the fractional escape rate values for ^{18}F-FDHR (Panels A and C) and ^{201}Tl (Panels B and D). The lines parallel to the flow axis map the effect of flow on fractional escape rate at only one point in time. These lines were obtained from linear regressions of FER(t) values generated by evaluating Equation 7 at selected time points using data from all 22 experiments. The lines parallel to the time axis map the effect of time on FER(t) at only one coronary flow and were obtained by connecting points on the FER(t)-vs.-flow regression lines.

Panels A and B display the effect of time and flow on ^{18}F-FDHR and ^{201}Tl fractional escape rate during the first 30 s after tracer introduction. The surfaces are composed of sixteen FER(t)-vs.-flow regression lines obtained at 2-s increments. FER(t) for ^{201}Tl was much greater than for ^{18}F-FDHR over all flows during the initial 30 s ($P < 0.0001$ for each time point). For both tracers, increasing flow resulted in higher FER(t) values for each point in time ($P < 0.02$ and $P < 0.002$ for ^{18}F-FDHR and ^{201}Tl, respectively). With flow held constant, there was a reduction in ^{201}Tl and ^{18}F-FDHR FER(t) values with time because of decreasing washout of activity from intermediate spectral components. Thallium-201 washout was very rapid at high flows early after tracer introduction. At low flows and after 15–20 s, the effects of time and flow were less prominent. Relative to ^{18}F-FDHR, flow exerted a much stronger effect on ^{201}Tl FER(t) during the first 20 s ($P < 0.05$ for each time point).

Panels C and D display surfaces composed of 16 FER(t)-vs.-flow regression lines obtained at 30 s and at 1 min increments from 1 min to 15 min. As was the case during the first 30 s, FER(t) values for ^{201}Tl were higher than those for ^{18}F-FDHR ($P < 0.001$ for each time point). Although less striking than immediately after isotope introduction, flow had a

stronger effect on ^{201}Tl FER(t) relative to that for ^{18}F-FDHR ($P < 0.05$ for each time point). Reflecting this difference, increasing flow rates increased ^{201}Tl FER(t) values at all time points ($P < 0.001$ for each time point) while ^{18}F-FDHR values were only intermittently increased (significant increases from 30 s to 3 min and from 7 min to 15 min [$P < 0.05$ for each time point]). With flow held constant, ^{18}F-FDHR and ^{201}Tl FER(t) declined with time because of decreasing washout of activity associated with intermediate spectral components.

^{18}F-FDHR and ^{201}Tl Retention

Figure 4 is a surface-plot of the effect of time and flow on ^{18}F-FDHR and ^{201}Tl net retention; its configuration is similar to Figure 3 except that the flow axis has been reversed to allow better visualization of the effect of flow on tracer retention. The 16 lines parallel to the flow axis are linear regressions of E_{net} values for all 22 experiments obtained by evaluating Equation 6 at 1-min increments. For both ^{18}F-FDHR and ^{201}Tl, the initial regression lines are identical to the lines in Figure 2 and represent initial extraction fraction with flow having a stronger effect on ^{18}F-FDHR than ^{201}Tl extraction fraction. For all subsequent time points, ^{18}F-FDHR net retention was greater than that for ^{201}Tl ($P < 0.0001$ for each time point), because of the larger FER(t) for ^{201}Tl. Increasing coronary flow reduced both ^{18}F-FDHR and ^{201}Tl net retention ($P < 0.0001$ for each tracer for each time point). Consistent with the different sensitivity to the effects of flow on washout, the decline for ^{201}Tl was steeper than ^{18}F-FDHR along the flow axis at times $t \geq 1$ min, indicating that flow had a greater effect on ^{201}Tl net retention ($P < 0.05$ for each time point).

^{18}F-FDHR and ^{201}Tl Uptake

Figure 5 is a surface-plot of the effect of time and flow on ^{18}F-FDHR and ^{201}Tl net uptake. The direction of the flow axis is identical to that of Figure 3. Since net uptake is computed as flow times E_{net} (Eq. 8), ideal flow tracers have an E_{net} of one at all times and flows. For such ideal perfusion tracers, this surface-plot would reduce to a two-dimensional graph with flow and net uptake values falling on the line of identity. As seen in Figures 2 and 4, neither ^{18}F-FDHR nor ^{201}Tl have an initial extraction fraction of one at any flow and the net retention of both tracers declines with increasing time and flow. Comparing the two agents, initial ^{18}F-FDHR uptake values were less linearly related to flow than those for ^{201}Tl, because initial extraction of ^{18}F-FDHR was sensitive to flow and initial extraction of ^{201}Tl was not (Fig. 2). However, ^{201}Tl retention dropped sharply during the first minute and was more sensitive to flow than that for ^{18}F-FDHR for the remainder of the 15-min experiment (Fig. 4). (At later times, ^{201}Tl uptake actually declines as flow increases. This is due to accelerated tracer washout at high flows in the absence of ^{201}Tl recirculation, a condition not encountered in vivo). Thus, after the first minute, ^{18}F-FDHR net uptake values were greater and more linearly related to flow than those for ^{201}Tl.

Figure 6 presents the relationship between net uptake and flow at one and fifteen minutes after tracer introduction for ^{18}F-FDHR and ^{201}Tl from the present study and comparable values for ^{125}I -iodorotenone and ^{99m}Tc-sestamibi from the previous investigation (*14*). Results for ^{18}F-FDHR and ^{201}Tl are shown in Panels A and C and ^{125}I -iodorotenone and ^{99m}Tc-sestamibi in Panels B and D. Comparing the areas under the uptake vs. flow curves at one minute (Panels A and B), the net uptakes for both ^{18}F-FDHR and ^{125}I-iodorotenone were closer to the line of identity than either of the clinically available tracers ($P < 0.0001$ for each comparison). There was a small but statistically significant difference in the areas under the uptake-vs. -flow curves for the two radiolabeled rotenone analogues at one minute after tracer injection, with the net uptake for ^{18}F-FDHR slightly closer to the line of identity than iodorotonone ($P < 0.05$).

At fifteen minutes after injection of isotopes (Panels C and D), net uptake of the two radiolabeled-rotenone analogues remained closer to the line of identity than either ^{201}Tl or ^{99m}Tc-sestamibi ($P < 0.0001$ for each comparison). Comparing ^{125}I-iodorotenone and ^{18}F-FDHR, the differences in areas under their uptake-vs. -flow curves were slightly greater than at one minute with the net uptake for ^{18}F-FDHR continuing to be closer to the line of identity than ^{125}I-iodorotonone ($P < 0.001$). These results indicate that both ^{18}F-FDHR and ^{125}I-iodorotenone were better flow tracers than either ^{201}Tl or ^{99m}Tc-sestamibi from one to fifteen minutes after bolus tracer introduction in the isolated rabbit heart. In addition, ^{18}F-FDHR was a slightly better flow tracer than ^{125}I-iodoroteone over the same time interval.

DISCUSSION

We compared ^{18}F-FDHR, a radiolabeled rotenone analogue, and ^{201}Tl as myocardial perfusion indicators in the isolated rabbit heart. We observed that ^{18}F-FDHR tissue tracer content was more closely related to flow than ^{201}Tl content except for a single measurement immediately after tracer introduction. Similarly, in previous work, we observed that tissue tracer content of another radiolabeled rotenone analogue, ^{125}I-iodorotenone, was more closely related to flow than ^{99m}Tc-sestamibi (*14*). When results from the two studies were combined, both ^{18}F-FDHR and ^{125}I-iodorotenone tissue tracer content were more closely related to flow than either ^{201}Tl or ^{99m}Tc-sestamibi. These observations indicate that ^{18}F-FDHR and ^{125}I-iodorotenone are better flow tracers than ^{201}Tl and ^{99m}Tc-sestamibi in the isolated rabbit heart.

RBC and Albumin Binding and Permeation of Capillary Wall

The initial extraction fraction of a tracer is frequently used to assess its ability to permeate the capillary wall (*21*). Usually, neutral lipophilic compounds readily escape from the capillary into the extravascular space since these compounds can diffuse through endothelial cell membranes (*5*). However, for ^{18}F-FDHR, the initial extraction was no greater than ^{201}Tl, a charged molecule that diffuses primarily through pores in the capillary wall (*21*). In addition, changes in flow affected ^{18}F-FDHR initial extraction fraction but failed to significantly alter it for ^{201}Tl. Since ^{18}F-FDHR binding to RBCs and albumin was virtually complete after 30 s of incubation, the most plausible explanation for these observations is that the rate-limiting step for ^{18}F-FDHR permeation of the capillary was dissociation from albumin and/or diffusion out of red blood cells.

Although infrequently cited in cardiac literature, binding of ^{201}Tl to RBCs has been extensively investigated (*22-24*) and it is well established that thallium enters the red blood cell's intracellular space and might not be available for exchange with the myocardium (*25*). In the present study, we observed that ^{201}Tl entered bovine RBCs slowly relative to ^{18}F-FDHR: 55% was associated with the red cell fraction at 15 min. These observations are consistent with our experience using ^{201}Tl in the red blood cell perfused rabbit heart. In a study comparing ^{201}Tl to ^{99m}Tc (*26*), we observed that the peak extraction for ^{201}Tl was 0.83 ± 0.06, a value similar to that observed in this investigation. In these two studies, the isotope injectate did not contain RBCs. However, in another investigation (*18*), the initial extraction fraction of ^{201}Tl was only 0.67 ± 0.07. In this latter study, the injectate contained RBCs. Since there was usually a lag time of up to 15 min between addition of ^{201}Tl to the RBC-containing perfusate and injection, there was sufficient time for ^{201}Tl to enter RBCs and be unavailable to the myocardium. Because this phenomenon has not been investigated in vivo, the effect of red cell sequestration on regional ^{201}Tl distribution/redistribution is not clear.

Since ^{201}Tl is charged, it has limited capillary permeability and is better extracted at low vs. high flows (*21, 27-29*). However, in both the current investigation and in a previously published report (*18*), the expected decline in thallium initial extraction fraction was not observed at higher coronary flows. There are two potential explanations for this anomalous behavior. First, at low flows, it takes longer to travel from the point of injection to myocardial capillaries so that there is increased time for thallium to be sequestered inside red blood cells. Since thallium inside red blood cells is not available to the myocardium, the expected increase in extraction fraction at low flows is not observed. Second, capillary permeability could increase as flow is increased due either to capillary recruitment or a temporal change in their "twinkling" pattern, both obviating a decline in extraction fraction at high flows. An apparent increase in capillary permeability at higher flows was observed by Weich et al. (*29*) when cardiac work was increased by rapid atrial pacing.

Washout and Retentions

The ability to separate intravascular from extravascular tracer distribution using spectral analysis allows a qualitative comparison of the rate-limiting steps of ^{18}F-FDHR vs. ^{201}Tl exchange between blood and myocardium. Early FER(t) provides a measure of the fraction of initially extracted tracer that back-diffuses into the intravascular space. In these experiments, early FER(t) for ^{201}Tl was much higher than that for ^{18}F-FDHR. Since the rate of diffusion out of the capillary was similar for these two tracers, the higher back-diffusion of ^{201}Tl is consistent with diminished sarcolemmal permeability relative to ^{18}F-FDHR. When this information is combined with the blood component binding studies and the two tracers are compared, the data suggest that diffusion of ^{18}F-FDHR into the myocyte is limited by dissociation from RBCs and/or albumin while ^{201}Tl is limited by sarcolemmal permeability.

At late times in these experiments, the escape of these two flow tracers is mostly related to diffusion out of the intracellular space. As with early FER(t), more ^{201}Tl escaped from the myocardium than ^{18}F-FDHR. Reflecting the less effective intracellular sequestration, ^{201}Tl retention was lower and more affected by flow than ^{18}F-FDHR at all times after the first measurement.

Although the superior retention of ^{18}F-FDHR is presumably related to abundant mitochondria in the myocardium (*10-13*), the intracellular binding characteristics of ^{18}F-FDHR (and ^{125}I-iodorotenone) have not been systematically evaluated in the heart. In addition, the effects of changes in mitochondrial metabolic rate due to altered workload, substrate supply, and ischemia are unknown. It is quite possible that extraction and retention of the radiolabeled rotenone analogues might be altered by changes in mitochondrial function, constraining their use as flow tracers.

Comparison to Other Positron-Emitting Flow Tracers

There are three positron-emitting flow tracers that are currently available for clinical use. ^{82}Rb is a generator-produced deposited flow tracer that does not require an on-site cyclotron. However, use of ^{82}Rb has been limited because it has a short half-life (75 s) and a high end-point energy that degrades image quality. Also, the kinetics of ^{82}Rb-myocardial deposition indicate that it is not as good a flow tracer as ^{201}Tl (*18*). In contrast to ^{82}Rb, ^{15}O-water is a flow-limited tracer with myocardial tracer delivery and washout determined by the rate of coronary flow. Qualitative estimation of regional perfusion is not possible from a single image: to estimate flow with ^{15}O-water, dynamic image acquisition is required and quantification of regional flow requires a tracer kinetic model.

^{13}N-ammonia is a deposited flow tracer that was initially used clinically to assess regional blood flow in 1972 (*30*) and has been shown to provide accurate qualitative assessment of regional myocardial perfusion directly from tomographic images (*31*). ^{13}N-ammonia has also been used to quantify regional flow (*32-37*), although the rapid appearance of ^{13}N-containing metabolites makes accurate assessment of the input function difficult. Previous studies evaluating ^{13}N-ammonia kinetics in vitro did not use the multiple indicator dilution technique (*38*), making comparison to the current results non-productive.

^{18}F-FDHR has two advantages compared to the positron-emitting flow tracers currently in use. First, both ^{15}O-water and ^{13}N-ammonia have short half-lives (2 min and 10 min, respectively) and require an on-site cyclotron. ^{18}F has a longer half-life (110 min) and does not require an on-site cyclotron; it can be obtained commercially. Second, ^{18}F has the potential of providing excellent image resolution relative to ^{82}Rb.

CONCLUSION

Combining results from this study and a previous investigation (*14*), ^{18}F-FDHR and ^{125}I-iodorotenone have been shown to be superior flow tracers relative to ^{201}Tl and ^{99m}Tc-sestamibi in the isolated rabbit heart. Although it is likely that these mitochondrial-avid tracers will be trapped in the myocardium of most mammalian species, there are issues that need further investigation. The first is that blood component binding might be different in patients than for bovine red blood cells and albumin. The second issue relates to potential changes in myocardial deposition when mitochondrial function is altered due to changes in workload, substrate supply, or development of ischemia. Although these issues need to be addressed, the clear superiority of ^{18}F-FDHR and ^{125}I-iodorotenone in the isolated rabbit heart compared to the tracers currently in use provides sufficient motivation to continue to evaluate rotenone analogues both in vitro and in vivo.

ACKNOWLEDGMENTS

This study was supported by National Heart, Lung, and Blood Institute Grants PO1 HL25840 and RO1 HL6087701 and by the Director, Office of Science, Office of Biological and Environmental Research (OBER), Medical Science Division of the United States Department of Energy under OBER contract DE–AC03–76SF00098.

REFERENCES

1. Shaw LJ, Iskandrian AE, Hachamovitch R, et al. Evidence-based risk assessment in noninvasive imaging. *J Nucl Med*. 2001;42:1424-1436.
2. Iskander S, Iskandrian AE. Risk assessment using single-photon emission computed tomographic technetium-99m sestamibi imaging. *J Am Coll Cardiol*. 1998;32:57-62.
3. Gibbons RJ, Chatterjee K, Daley J, et al. ACC/AHA/ACP-ASIM guidelines for the management of patients with chronic stable angina: a report of the American College of Cardiology/American Heart Association Task Force on Practice Guidelines (Committee on Management of Patients With Chronic Stable Angina). *J Am Coll Cardiol*. 1999;33:2092-2197.
4. Alpert JS. Defining myocardial infarction: "will the real myocardial infarction please stand up?" *Am Heart J*. 2003;146:377-379.
5. Bassingthwaighte JB, Raymond GM, Chan JI. Principles of tracer kinetics. In: Zaret BL, Beller GA. *Nuclear Cardiology: State of the Art and Future Directions*. St. Louis: Mosby-Year Book, Inc., 1993:3-23.
6. Yoshinaga K, Katoh C, Noriyasu K, et al. Reduction of coronary flow reserve in areas with and without ischemia on stress perfusion imaging in patients with coronary artery disease: a study using oxygen 15-labeled water PET. *J Nucl Cardiol*. 2003;10:275-283.
7. Bergmann SR, Fox KA, Rand AL, et al. Quantification of regional myocardial blood flow in vivo with $H_2{}^{15}O$. *Circulation*. 1984;70:724-733.
8. Bergmann SR, Herrero P, Markham J, Weinheimer CJ, Walsh MN. Noninvasive quantitation of myocardial blood flow in human subjects with oxygen-15-labeled water and positron emission tomography. *J Am Coll Cardiol*. 1989;14:639-652.
9. Araujo LI, Lammertsma AA, Rhodes CG, et al. Noninvasive quantification of regional myocardial blood flow in coronary artery disease with oxygen-15-labeled carbon dioxide inhalation and positron emission tomography. *Circulation*. 1991;83:875-885.
10. Ueno H, Miyoshi H, Ebisui K, Iwamura H. Comparison of the inhibitory action of natural rotenone and its stereoisomers with various NADH-ubiquinone reductases. *Eur J Biochem*. 1994;225:411-417.
11. Ueno H, Miyoshi H, Inoue M, Niidome Y, Iwamura H. Structural factors of rotenone required for inhibition of various NADH-ubiquinone oxidoreductases. *Biochim Biophys Acta*. 1996;1276:195-202.
12. Greenamyre JT, Higgins DS, Eller RV. Quantitative autoradiography of dihydrorotenone binding to complex I of the electron transport chain. *J Neurochem*. 1992;59:746-749.
13. Ramsay RR, Krueger MJ, Youngster SK, Gluck MR, Casida JE, Singer TP. Interaction of 1-methyl-4-phenylpyridinium ion (MPP^+) and its analogs with the rotenone/piericidin binding site of NADH dehydrogenase. *J Neurochem*. 1991;56:1184-1190.
14. Marshall RC, Powers-Risius P, Reutter BW, et al. Kinetic analysis of ^{125}I-iodorotenone as a deposited myocardial flow tracer: comparison with ^{99m}Tc-sestamibi. *J Nucl Med*. 2001;42:272-281.
15. Chinnard FP, Vosburgh GJ, Enns T. Transcapillary exchange of water and of other substances in certain organs of the dog. *Am J Physiol*. 1955;183:221–234.
16. Cunningham VJ, Jones T. Spectral analysis of dynamic PET studies. *J Cereb Blood Flow Metab*. 1993;13:15-23.
17. Marshall RC. Correlation of contractile dysfunction with oxidative energy production and tissue high energy phosphate stores during partial coronary flow disruption in rabbit heart. *J Clin Invest*. 1988;82:86-95.
18. Marshall RC, Taylor SE, Powers-Risius P, et al. Kinetic analysis of rubidium and thallium as deposited myocardial blood flow tracers in isolated rabbit heart. *Am J Physiol*. 1997;272:H1480-1490.

19. Millar WT, Smith JFB. Protein iodination using IODO-GEN. *Int J Appl Radiat Isot*. 1983;34:639-641.
20. Kendall M, Stuart A. *The Advanced Theory of Statistics*. New York: Oxford University Press, 1979.
21. Bassingthwaighte JB, Goresky CA. Modeling in the analysis of solute and water exchange in the microvasculature. In: Renkin EM, Michel CC. *Handbook of Physiology, sect 2, The Cardiovascular System, vol IV, The Microcirculation*. Bethesda, Maryland: American Physiological Society, 1984:549-626.
22. Sands H, Delano ML, Camin LL, Gallagher BM. Comparison of the transport of $^{42}K^+$, $^{22}Na^+$, $^{201}Tl^+$, and $[^{99m}Tc(dmpe)_2 X Cl_2]^+$ using human erythrocytes. *Biochim Biophys Acta*. 1985;812:665-670.
23. Skullskii IA, Manninen V. Effect of membrane potential on the passive transport of Tl^+ in human red blood cells. *Acta Physiol Scand*. 1981;111:343-348.
24. Skulskii IA, Manninen V, Glasunov VV. Thallium and rubidium permeability of human and rat erythrocyte membrane. *Gen Physiol Biophys*. 1990;9:39-44.
25. Goresky CA, Bach GG, Nadeau BE. Red cell carriage of label. *Circ Res*. 1975;36:328-351.
26. Marshall RC, Leidholdt EM, Jr., Zhang DY, Barnett CA. Technetium-99m hexakis 2-methoxy-2-isobutyl isonitrile and thallium-201 extraction, washout, and retention at varying coronary flow rates in rabbit heart. *Circulation*. 1990;82:998-1007.
27. Bassingthwaighte J, Winkler B, King R. Potassium and thallium uptake in dog myocardium. *J Nucl Med*. 1997;38:264-274.
28. Melin JA, Becker LC. Quantitative relationship between global left ventricular thallium uptake and blood flow: effects of propranolol, ouabain, dipyridamole, and coronary artery occlusion. *J Nucl Med*. 1986;27:641-652.
29. Weich HF, Strauss HW, Pitt B. The extraction of thallium-201 by the myocardium. *Circulation*. 1977;56:188-191.
30. Harper PV, Lathrop KA, Krizek H, Lembares N, Stark V, Hoffer PB. Clinical feasibility of myocardial imaging with $^{13}NH_3$. *J Nucl Med*. 1972;13:278-280.
31. Schelbert HR, Wisenberg G, Phelps ME, et al. Noninvasive assessment of coronary stenoses by myocardial imaging during pharmacologic coronary vasodilation. VI. Detection of coronary artery disease in human beings with intravenous N-13 ammonia and positron computed tomography. *Am J Cardiol*. 1982;49:1197-1207.
32. Hutchins GD, Schwaiger M, Rosenspire KC, Krivokapich J, Schelbert H, Kuhl DE. Noninvasive quantification of regional blood flow in the human heart using N-13 ammonia and dynamic positron emission tomographic imaging. *J Am Coll Cardiol*. 1990;15:1032-1042.
33. Krivokapich J, Smith GT, Huang SC, et al. ^{13}N ammonia myocardial imaging at rest and with exercise in normal volunteers. Quantification of absolute myocardial perfusion with dynamic positron emission tomography. *Circulation*. 1989;80:1328-1337.
34. Kuhle WG, Porenta G, Huang SC, et al. Quantification of regional myocardial blood flow using 13N-ammonia and reoriented dynamic positron emission tomographic imaging. *Circulation*. 1992;86:1004-1017.
35. Beanlands RS, deKemp R, Scheffel A, et al. Can nitrogen-13 ammonia kinetic modeling define myocardial viability independent of fluorine-18 fluorodeoxyglucose? *J Am Coll Cardiol*. 1997;29:537-543.
36. Muzik O, Beanlands RS, Hutchins GD, Mangner TJ, Nguyen N, Schwaiger M. Validation of nitrogen-13-ammonia tracer kinetic model for quantification of myocardial blood flow using PET. *J Nucl Med*. 1993;34:83-91.

37. Gerber BL, Melin JA, Bol A, et al. Nitrogen-13-ammonia and oxygen-15-water estimates of absolute myocardial perfusion in left ventricular ischemic dysfunction. *J Nucl Med.* 1998;39:1655-1662.
38. Krivokapich J, Huang SC, Phelps ME, MacDonald NS, Shine KI. Dependence of $^{13}NH_3$ myocardial extraction and clearance on flow and metabolism. *Am J Physiol.* 1982;242: H536-542.

TABLE 1. Spectral Analysis Components of ^{18}F-FDHR and ^{201}Tl

		Component				
		Undelayed	Intermediate		Slow	
Tracer	Percentile	c_0	$c_{1,\ldots,m-1}$	$t_{1,\ldots,m-1}$	c_m	t_m
^{18}F-FDHR	75	0.20	0.14	3.7	1.1	190*
^{18}F-FDHR	50	0.14	0.11	2.8	0.55	190*
^{18}F-FDHR	25	0.09	0.09	2.0	0.31	82
^{201}Tl	75	0.17	0.39	3.8	0.95	130
^{201}Tl	50	0.14	0.24	0.92	0.64	28
^{201}Tl	25	0.08	0.19	0.19	0.56	19

*Slow component has artificial upper limit imposed by spectral analysis, which fitted components having mean transit delay times ranging from 1 s to 190 min.

Data represent upper quartile, median, and lower quartile (75^{th}, 50^{th}, and 25^{th} percentile) values for fractions and mean transit delay times for spectral model impulse response components for 22 experiments. Fractions and mean transit delay time for intermediate components have been combined with use of Equation 5. Fractions c_0, $c_{1,\ldots,m-1}$, and c_m are dimensionless. Units for mean transit delay times $t_{1,\ldots,m-1}$ and t_m are minutes.

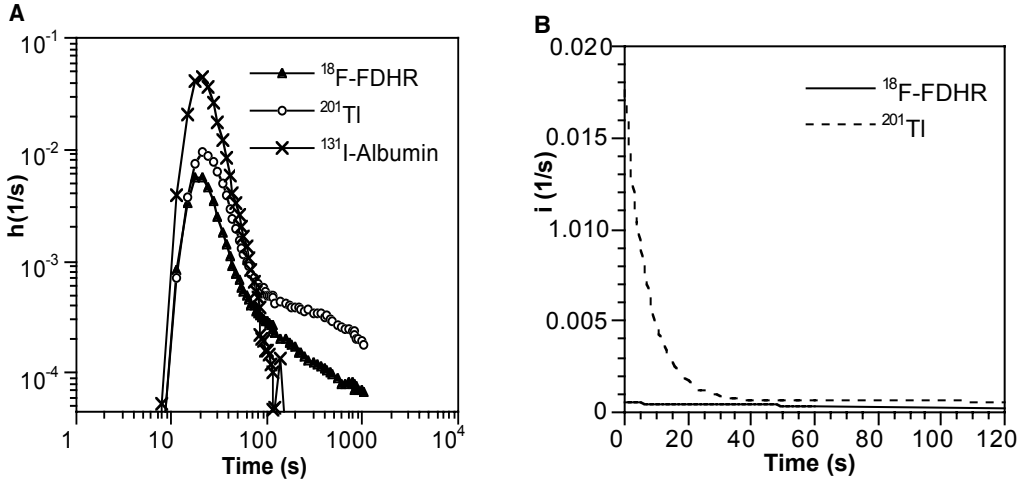

FIGURE 1. (A) Fractional venous appearance rate, h(t), of ^{18}F-FDHR, ^{201}Tl, and ^{131}I-albumin as function of venous collection time. (B) Delayed components of the deconvolved impulse response function, i(t), for the first 120 s. Both data sets are from the same experiment; the coronary flow rate was 1.6 mL/min/g of LV wet weight.

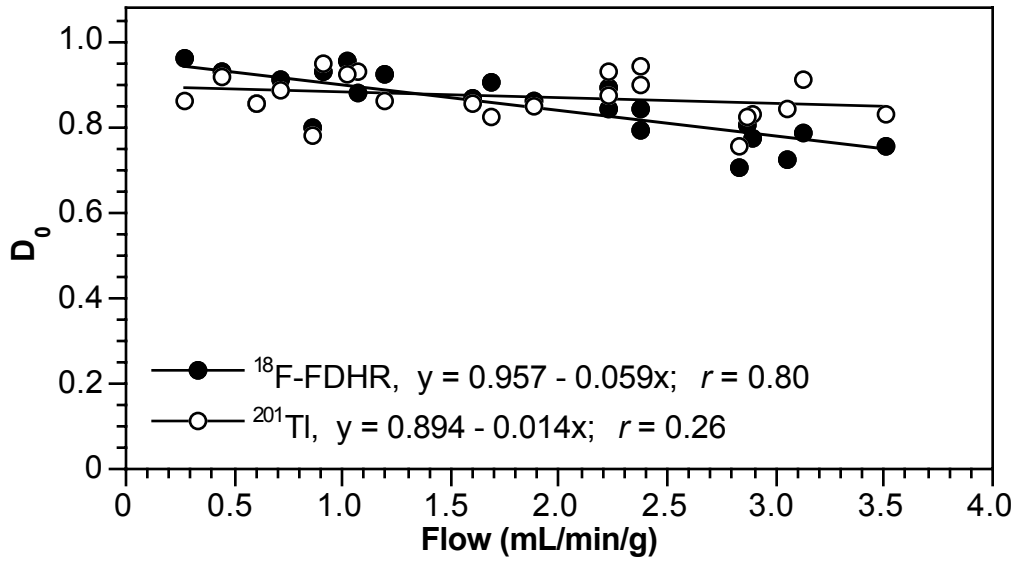

FIGURE 2. Initial extraction fraction of ^{18}F-FDHR and ^{201}Tl as a function of blood flow. Data were pooled from 22 experiments, with each data point representing a single experiment. Equations for the linear fits to data points are shown.

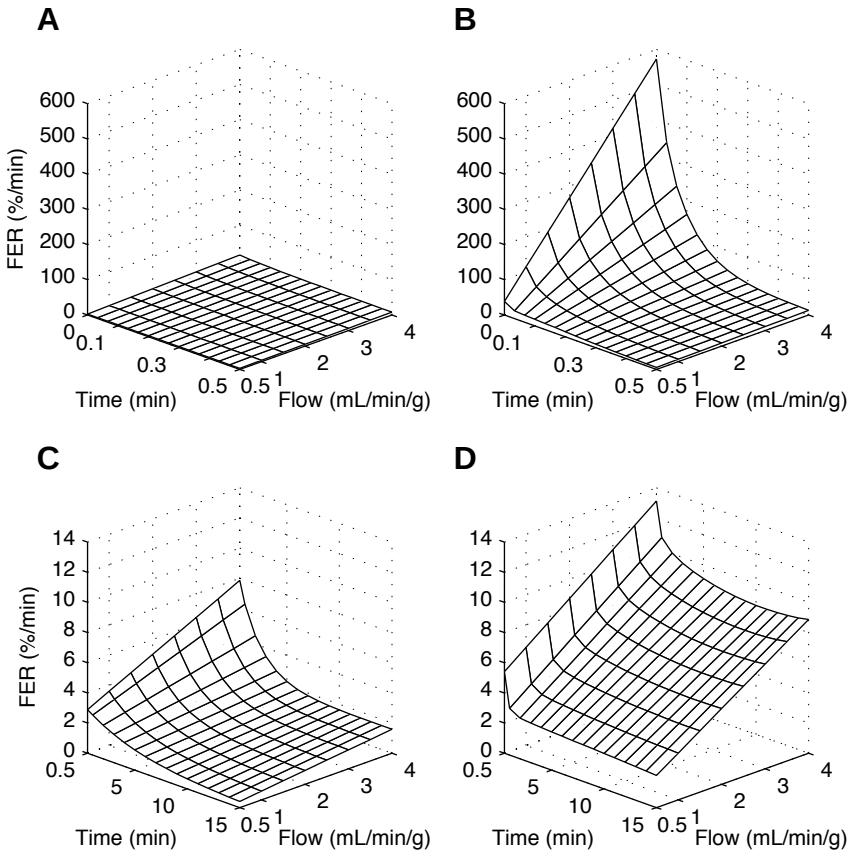

FIGURE 3. FER(t) as a function of flow and time for ^{18}F-FDHR (A and C) and ^{201}Tl (B and D) during the first 30 s (A and B) and from 30 s to 15 min (C and D).

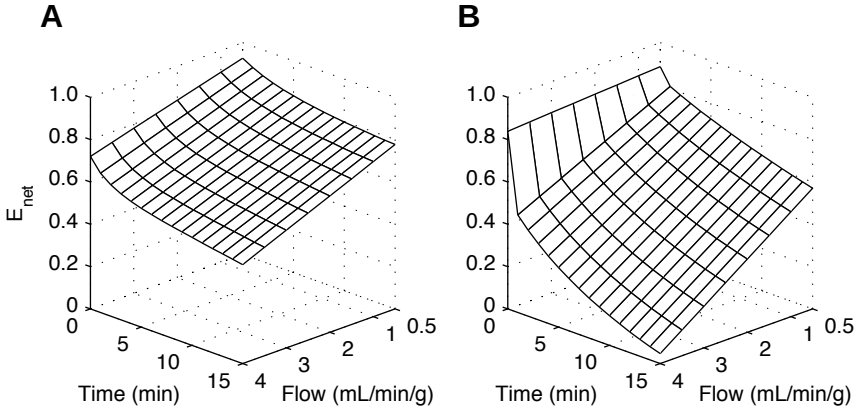

FIGURE 4. E_{net}(t) as a function of flow and time for ^{18}F-FDHR (A) and ^{201}Tl (B).

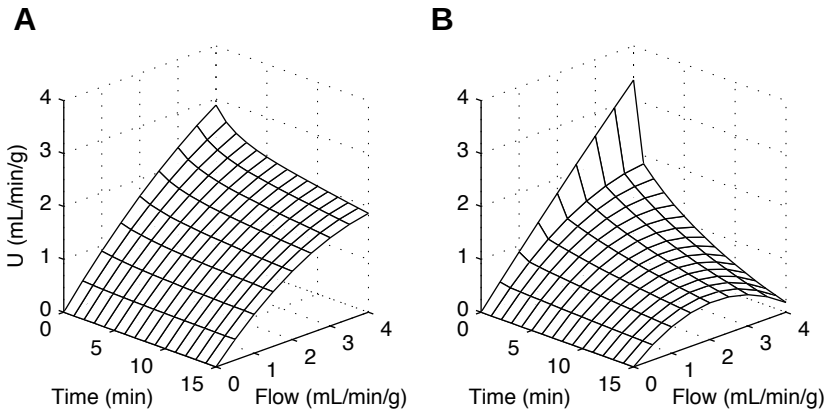

FIGURE 5. U(t) as a function of flow and time for ^{18}F-FDHR (A) and ^{201}Tl (B).

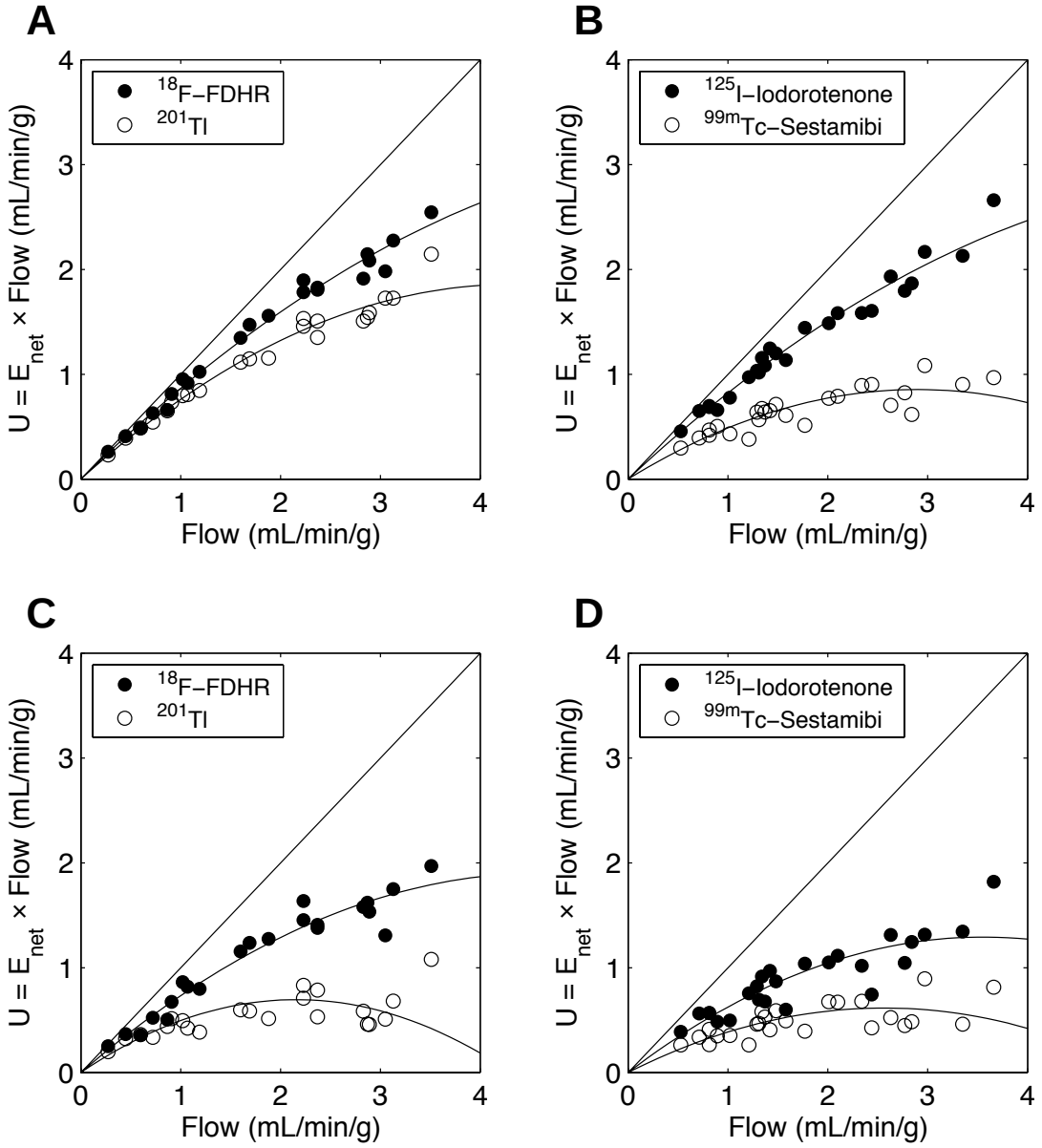

FIGURE 6. Relationship between net uptake, U(t), and flow for ^{18}F-FDHR and ^{201}Tl (A and C) and ^{125}I-iodorotenone and ^{99m}Tc-sestamibi (B and D) at 1 min (A and B) and 15 min (C and D).